Available online at www.sciencedirect.com
SCIENCE DIRECT
Journal of Catalysis 230 (2005) 237–248
JOURNAL OF CATALYSIS
www.elsevier.com/locate/jcat

Enhanced soot oxidation by lattice oxygen via La^{3+}-doped CeO_2

A. Bueno-López, K. Krishna, M. Makkee *, J.A. Moulijn

Reactor & Catalysis Engineering, DelftChemTech, Delft University of Technology, Julianalaan 136, NL 2628 BL Delft, The Netherlands

Received 14 September 2004; revised 12 November 2004; accepted 24 November 2004

Abstract

The catalytic behaviours of CeO_2 and a series of La^{3+}-doped CeO_2 catalysts (La^{3+} loading between 5 and 50 wt%) have been studied for soot oxidation by O_2. XRD and Raman spectroscopy characterisation indicated that solid solutions are formed in the studied Ce/La ratio, in which La^{3+} cations replace Ce^{4+} cations in the CeO_2 lattice. Thermogravimetric analysis showed that La^{3+} significantly improves CeO_2 catalytic activity for soot oxidation with O_2. The best catalytic activity was found with 5 wt% La^{3+}-doped CeO_2 catalyst (CeO_2-5La), in both loose and tight contact conditions. This improvement seems to be related to the increase in BET surface area and the change in the catalyst redox properties of CeO_2 brought about by doping with La^{3+}. La^{3+} decreases the onset temperature of Ce^{4+} to Ce^{3+} reduction by H_2 from 580 °C (CeO_2) to 325 °C (CeO_2-5La) and increases the amount of Ce^{4+} that can be reduced by H_2 (maximum amount for CeO_2-5La catalyst).

An advanced TAP reactor is used for the first time to study catalysed soot oxidation with labelled oxygen. In the absence of catalyst, oxidation starts above 500 °C, and mainly labelled oxidation species (CO and CO_2) were found. In the presence of catalyst, it is shown that the gas-phase labelled oxygen replaces nonlabelled lattice oxygen, creating the highly active nonlabelled oxygen. This highly active nonlabelled oxygen reacts with soot, giving CO and CO_2. The creation of such active oxygen species starts from 400 °C and thereby decreases the soot oxidation temperature. CeO_2-5La produces more such active species, for example, leading to 98% oxygen conversion at 400 °C compared with 37% over CeO_2 alone under identical circumstances.

Keywords: Active oxygen; Catalysed soot oxidation; Ceria; Lanthana; Oxygen exchange; Solid solution; Soot; Temporal analysis of products

1. Introduction

Air quality is an environmental problem that must be tackled by today's society [1]. Although the quality of air in urban areas is improving, in spite of growing urbanisation, because of increasing human mobility and, therefore, the increasing number of vehicles in our cities, still further improvement is needed.

The most used internal combustion engines in vehicles are the Otto and Diesel engines. The combustion processes occurring in these engines are almost 100% complete. However, some undesirable by-products are formed. Otto engines, running on gasoline, generate mainly CO, hydrocarbons (HC), and NO_x, whereas diesel engines produce small-size carbon particles (soot), NO_x, and small amounts of CO and HC.

Diesel exhaust gases had traditionally been considered clean in comparison with the exhaust gases of gasoline vehicles [2], but the successful introduction of three-way catalyst (TWC) for use in gasoline-powered vehicles and the development of modern engines have changed this benefit of diesel engines. Therefore, the search for particulate and NO_x reduction techniques is an issue of current scientific and technological research.

The conventional TWC used in gasoline engines converts simultaneously the HC, CO, and NO_x present in the exhaust gas into H_2O, CO_2, and N_2. Typical TWC formulations combine very active noble metals such Pd, Rh, or Pt on an oxygen storage component, generally based on rare earth oxides [3]. The optimal performance of these catalysts

* Corresponding author. Fax: +31-15-278-5006.
E-mail address: m.makkee@tnw.tudelft.nl (M. Makkee).

0021-9517/$ – see front matter
doi:10.1016/j.jcat.2004.11.027

is reached when the exhaust gas is present in a stoichiometric air/fuel ratio (14.6:1). However, the gas composition oscillates slightly around this ratio, and the buffer properties of the rare earth component permit the storage of oxygen during fuel-poor periods (net oxidising) and supply additional oxygen during fuel-rich periods (net reducing). Automotive pollution control is the most important application of rare earth oxides today [4]. The main properties of rare earth oxides for this TWC application are (i) a large oxygen storage capacity via the redox process $Ce^{4+} \leftrightarrow Ce^{3+}$; (ii) improvement of noble metals dispersion; (iii) improvement of the thermal stability of supports; and (iv) promotion of the water–gas shift reaction [5].

A catalytic device like TWC is not available for NO_x and soot elimination in diesel exhaust gases, in spite of the great advances that have been made in the last years in diesel particulate-trapping techniques [6]. Because of the lean-burn conditions in the diesel engine, NO_x reduction can only be performed via selective catalytic reduction with urea or hydrocarbon as a reductant. The main problem of soot elimination is that the onset temperature for soot combustion catalysts ($> 500\,^{\circ}C$) is too high for spontaneous regeneration of the filters, and, therefore, it is necessary to ignite soot periodically by raising the temperature with or without diesel fuel addition [7]. This technology is commercially available for soot abatement. Another technical approach is the oxidation of soot with NO_2 (NO_2 is converted from NO), which is much more reactive than O_2 [6,8]. Strategies for the reutilisation of NO in several cycles have also been developed [9]. Recently it has been found that CeO_2 has the potential to increase the oxidation rate of soot, because of the creation of "active oxygen" [10]. This finding opens a new route for the development of soot oxidation catalysts based on these species. The generation and feasible utilisation of highly reactive "active oxygen" for soot oxidation is a focus of ongoing investigation.

Despite the fact that CeO_2 and CeO_2-based solid solutions containing different rare earth metals have been extensively studied for TWC application [3,4], few detailed studies have analysed the utilisation of these materials for soot oxidation [11,12].

In this study, La^{3+}-doped CeO_2 catalysts have been prepared and tested for soot oxidation, and their activity has been compared with that of CeO_2. In this paper we present results for (i) the preparation of La^{3+}-containing CeO_2 solid solutions with different Ce/La ratios; (ii) the catalytic activity of these materials for soot oxidation by O_2; (iii) the characterisation of the crystalline structure, surface area, and redox properties of these materials, which will provide information about the key factors that control the catalytic activity of these materials for soot oxidation; and (iv) study of the interaction of O_2 with catalysts and soot-catalyst mixtures in an advanced TAP reactor with the use of normal and labelled O_2, which provides information about the role of "active oxygen" species in the O_2 soot oxidation reaction.

2. Experimental

2.1. Catalyst preparation

Nine catalysts have been prepared, one pure CeO_2 catalyst and eight La^{3+}-containing CeO_2 catalysts. La^{3+}-containing catalysts were denoted as CeO_2-%La, where % stands for the target La^{3+} percentage, determined by the formula $\% = (100 \cdot g_{La})/(g_{Ce} + g_{La})$. The CeO_2 catalyst was denoted as CeO_2.

$Ce(NO_3)_3 \cdot 6H_2O$ (Aldrich, 99%) and $La(NO_3)_3 \cdot 6H_2O$ (Merck, 99%) were used as precursors for catalyst preparation. The required amounts of these precursors were physically mixed in a mortar and were thermally treated in a furnace at $1000\,^{\circ}C$ for 90 min in air (heating rate $10\,^{\circ}C/min$).

2.2. Characterisation

The BET surface areas of catalysts were determined by physical adsorption of N_2 at $-196\,^{\circ}C$ in an automatic volumetric system (Autosorb-6, Quantachrome).

Temperature-programmed reduction by H_2 (TPR) was carried out in a tubular quartz reactor (inner diameter 5 mm) coupled to a TCD analyser for monitoring H_2 consumed. In the experiments the sample (50 mg of fresh catalyst) was heated at $10\,^{\circ}C/min$ from room temperature to $1000\,^{\circ}C$ in 30 ml/min flow of 7.7 vol% H_2 in Ar. To quantify the total amount of H_2 consumed during the experiments, CuO was used as a calibration reference.

Raman spectra were recorded in a Renishaw Raman imaging microscope (system 2000) with a 20-mW Ar laser (514 nm). The Raman microscope was calibrated with the use of a silicon wafer.

X-ray diffractograms were recorded with a Philips X-ray diffractometer (PW 1840) using Ni-filtered Cu-K_α radiation ($\lambda = 0.15418$ nm).

Temporal analysis of products (TAP) was used to analyse the interaction between gas-phase O_2 and selected catalysts (CeO_2 and CeO_2-5La) at temperatures between 200 and $600\,^{\circ}C$ in the so-called Multitrack system, with labelled and nonlabelled oxygen. A small cylindrical reactor (7 mm i.d.) containing the catalyst was connected to an ultrahigh vacuum system (10^{-6} Pa). Small gas pulses, typically consisting of $\sim 10^{16}$ molecules of pure oxygen, were fed to the catalyst with high-speed gas pulsing valves. The reactor was coupled to three mass spectrometers that were able to measure the components of the gas leaving the reactor with a maximum sampling frequency of 1 MHz. In a separate experiment Ar gas was pulsed through the catalyst bed at different temperatures, and it can be assumed that it did not interact chemically with the catalyst. Therefore, the Ar response profile is a reference for noninteracting gas. Comparison of the Ar and O_2 responses shows the extent of the interaction. The oxygen pulse experiments were carried out with 100 mg of catalyst (around 10^{20} molecules of CeO_2), and this amount is much higher than the amount of gas molecules pulsed. At

least 10^4 O_2 pulses are necessary to reach similar molecular amounts of catalyst. Therefore, it is assumed that the small number of labelled oxygen pulses used in studying its interaction at each temperature do not change the nature of the catalyst.

The first step of the experiment consisted of stabilisation of temperature at 200 °C in vacuum and pulsing of nonlabelled O_2 until oxygen uptake by the catalyst was no longer observed. The steady state was reached within about 125 pulses. Subsequently, the temperature was increased to 300, 400, 500, and 600 °C, and nonlabelled O_2 was pulsed at each temperature. Above 200 °C, oxygen uptake was not observed after 25 pulses, as the catalyst was already saturated. Once the above experiments were performed, the temperature was decreased to 200 °C and stabilised, and the same set of experiments was carried out with pure labelled O_2 ($^{18}O_2$, $< 1\%$ $^{16}O_2$ impurity).

Experiments similar to those described above were carried out with 10 mg of soot, and 10 mg of soot mixed with 100 mg of selected catalysts (CeO_2 and CeO_2-5La) in tight contact. In these experiments, only labelled O_2 was pulsed.

2.3. Soot oxidation activity in TGA

The catalysed soot oxidation was studied in a thermogravimetric analyser (TGA, Mettler Toledo, TGA/SDTA851[e]). Oxidation experiments consisted of heating the soot–catalyst mixtures at 10 °C/min from 30 to 800 °C in a 100 ml/min flow of air. The soot/catalyst weight ratio was 1:4. Because contact between soot and catalyst is a key factor in this process [13], experiments in *loose* and *tight contact* conditions were performed. For loose contact experiments, soot and catalyst were mixed with a spatula, whereas for tight contact tests the two components were intimately mixed in a mortar.

The model soot used in this study was a carbon black from Degussa S.A. (Printex-U). Table 1 compiles some physicochemical properties of this model soot.

Table 1
Model Printex-U soot characterisation (data from [8])

Fraction of adsorbed hydrocarbons	5.2%
Ash	< 0.1%
BET surface area	95 m^2/g
CHNS analysis	92.2% C
	0.6% H
	0.2% N
	0.4% S

3. Results

3.1. Soot oxidation activity

Fig. 1 shows the parameter $T_{50\%}$ (the temperature at which 50% of soot is converted) from TGA experiments under both loose and tight contact conditions. The $T_{50\%}$ temperature for noncatalysed soot oxidation is 613 °C under the experimental conditions used. As expected, CeO_2 decreases this temperature to 605 and 575 °C for loose and tight contact conditions, respectively. The presence of La^{3+} in the catalysts significantly improves the catalytic behaviour of CeO_2 when it is in tight contact with soot and to a small extent in loose contact experiments. The best activity was obtained with the catalyst CeO_2-5La ($T_{50\%} = 589$ and 410 °C for loose and tight contact, respectively). In loose contact conditions, the $T_{50\%}$ temperature of the samples CeO_2-40La and CeO_2-50La is similar to that observed for pure CeO_2. However, for tight contact experiments, the whole series of La^{3+}-containing samples shows better catalytic activity than CeO_2. Note that the catalytic behaviour of a physical mixture of the oxides $CeO_2 + La_2O_3$ is significantly lower than that of the sample CeO_2-5La.

Fig. 1 shows that the contact between soot and catalyst drastically affects the oxidation temperature, which is in accordance with the observations of Van Setten et al. [13]. In spite of loose contact experiments that provide more realistic information on catalyst behaviour under real operating conditions [13], tight contact experiments were useful for an

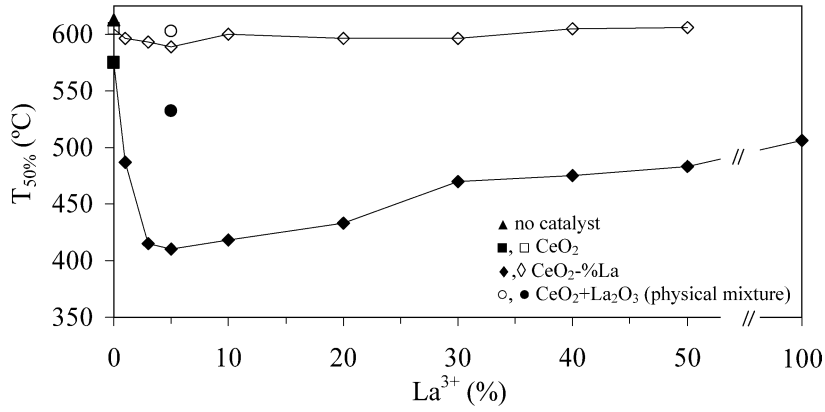

Fig. 1. Soot oxidation by O_2 in TGA. Open symbols: loose contact; solid symbols: tight contact. $T_{50\%}$ is the temperature at which 50% soot is converted. (Line to guide the eyes.)

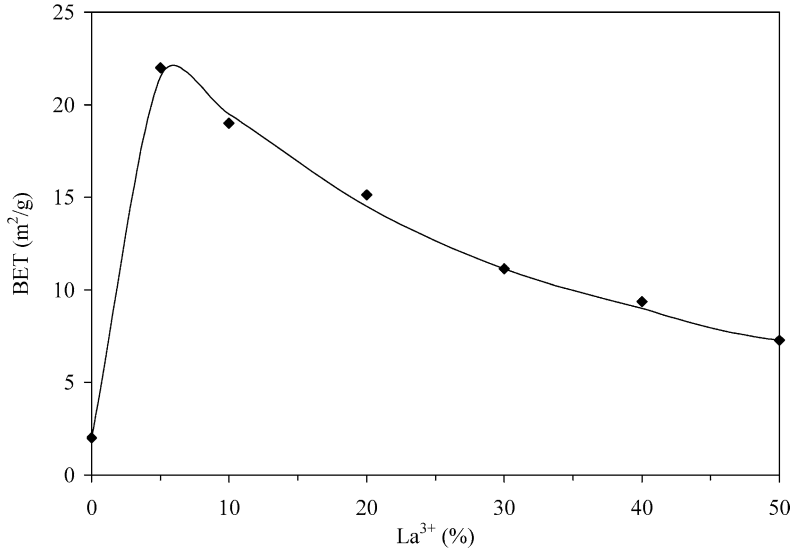

Fig. 2. BET surface area of CeO_2-%La with varying La^{3+} doping. (Line to guide the eyes.)

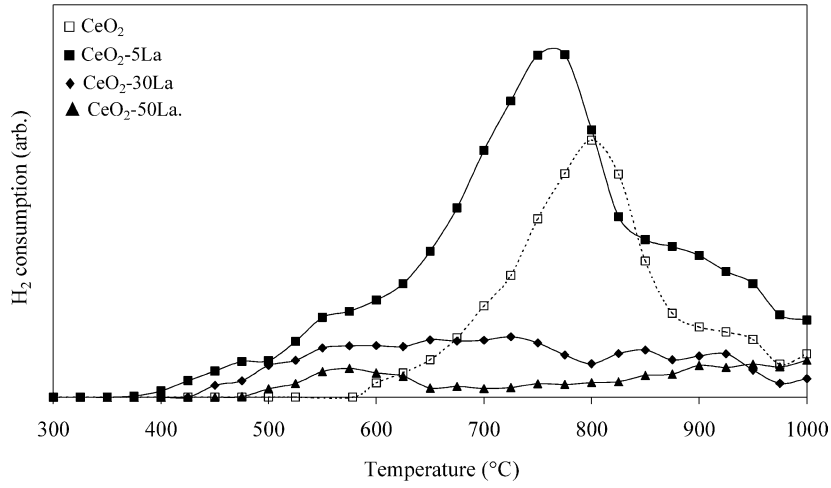

Fig. 3. H_2 consumption profiles during TPR of CeO_2 and CeO_2-%La catalysts.

analysis of the differences in the catalytic activity of the set of samples tested in this study.

3.2. Surface area

The BET surface areas of catalysts are presented in Fig. 2. The low surface area of CeO_2 (about 3 m^2/g) is reasonable, considering that the samples were prepared by thermal treatment at high temperature (1000 °C) [14]. La^{3+} improves the BET surface area of CeO_2, and a maximum value of 22 m^2/g is reached by the sample CeO_2-5La. This finding is in agreement with data reported by Vidmar et al. [15], who studied the effect of trivalent dopants on the properties of $Ce_{0.6}Zr_{0.4}O_2$ mixed oxides. These authors observed that La^{3+} and Y^{3+} incorporation into $Ce_{0.6}Zr_{0.4}O_2$ mixed oxides increases the surface area of these materials.

Note that the BET surface area of the catalyst in Fig. 2 follows a trend that is the inverse of that observed in Fig. 1 for the parameter $T_{50\%}$, that is, the higher the BET surface area, the lower the soot oxidation temperature. This relationship is discussed in more detail in Section 4.

3.3. TPR

TPR experiments were performed to analyse the redox properties of the fresh catalysts; H_2 consumption profiles for selected samples are shown in Fig. 3.

It is generally accepted [16] that two peaks characterise the reduction profile of pure CeO_2. The first peak, at about 425 °C, is attributed to the reduction of the uppermost layers of Ce^{4+}, and the main peak, at about 800 °C, originates with the reduction of the bulk. However, in the CeO_2 profile in Fig. 3 only the bulk peak is observed, which is reasonable when we consider that the BET surface area of this sample is very low (3 m^2/g). In contrast, the profile of the catalyst CeO_2-5La shows a shoulder at lower temperatures (375–650 °C). If we take into account that the BET surface area of this sample is 22 m^2/g, this shoulder could be attributed to

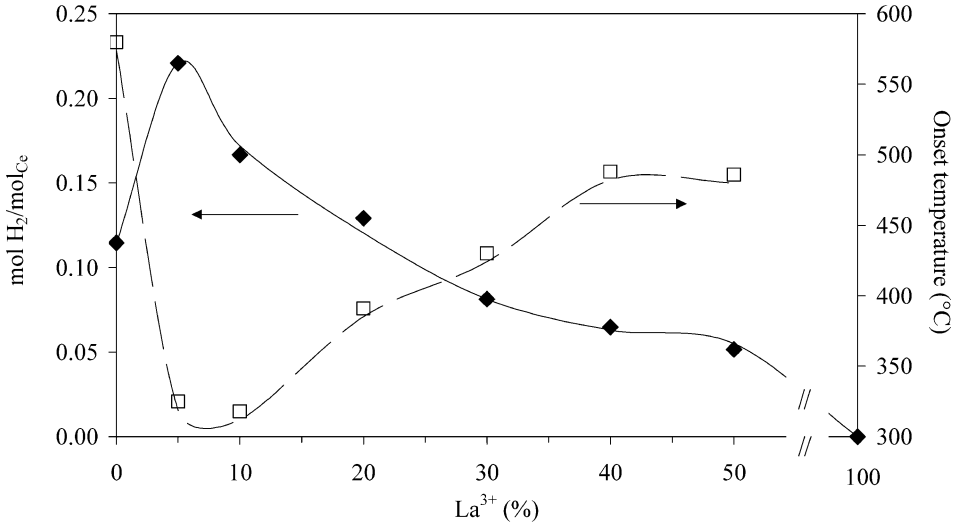

Fig. 4. Total H_2 consumption and onset temperature of H_2 consumption during TPR over CeO_2 and CeO_2-%La catalysts with varying La^{3+} contents. (Line to guide the eyes.)

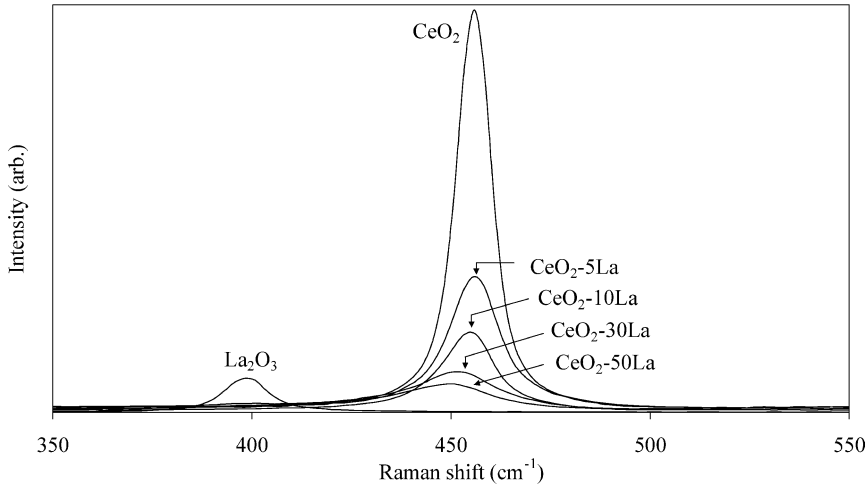

Fig. 5. Raman spectra of CeO_2 and CeO_2-%La catalysts.

surface reduction of Ce^{4+} in the CeO_2-5La catalyst. Moreover, the bulk reduction temperature of CeO_2-5La decreases and approaches the surface reduction peak. The generally accepted explanation for this is that the surface and bulk reductions occur concurrently [16]. Comparison between CeO_2 and CeO_2-5La profiles shows that La^{3+} decreases the onset temperature of Ce^{4+} reduction and increases the amount of Ce^{4+} that can be reduced (Fig. 4). However, the amount of Ce^{4+} reduced on samples CeO_2-30La and CeO_2-50La decreases significantly in comparison with CeO_2-5La. This is expected if we consider the fact that the higher the La^{3+} loading, the lower the amount of Ce^{4+}.

The total amounts of H_2 consumed during TPR were quantified; these are shown in Fig. 4. In this figure, the onset temperatures have also been included. The highest amount of H_2 is consumed by the sample CeO_2-5La, which is also the most active catalyst in soot oxidation. This sample also shows the lowest onset temperature of H_2 consumption.

3.4. Raman spectroscopy characterisation

The Raman spectroscopy technique has been used for the investigation of fresh catalysts structure; the spectra obtained are compiled in Fig. 5. For comparison, the Raman spectrum of La_2O_3 is also included in this figure.

The spectra in Fig. 5 corresponding to CeO_2-%La catalysts do not present the typical La_2O_3 band, which suggest that La^{3+} is located in the CeO_2 lattice. The main band of CeO_2 and CeO_2-%La catalysts at 459 cm^{-1} is the only allowed Raman mode (F_{2g}) of fluorite-type structure [17,18]. Fluorite-structure is a cubic structure (fcc) in which the cations are placed in the corners and in the centres of faces and oxygen atoms are located at the tetrahedral sites. The Raman spectra for these fluorite-type oxide structures are dominated by oxygen lattice vibrations and are sensitive to crystalline symmetry [19]. The presence of La^{3+} in the CeO_2 lattice deforms the structure, and the fluorite-characteristic peak intensity decreases significantly

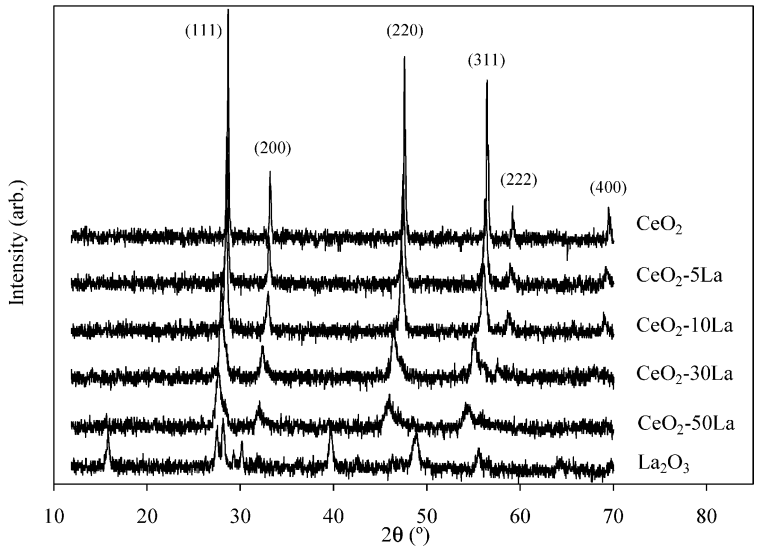

Fig. 6. X-ray diffractograms of CeO_2 and CeO_2-%La catalysts.

with La^{3+} loading. It has been reported that this deformation favours oxygen mobility, affecting the redox behaviour of the material [20], which is consistent with our TPR results.

3.5. XRD characterisation

Powder X-ray diffractograms for the fresh CeO_2 and CeO_2-%La catalysts are shown in Fig. 6. X-ray diffraction patterns confirm that the La^{3+}-containing catalysts present the true mixed-oxide phase with the cubic, fluorite-type structure typical of CeO_2. All of the diffractograms contain the six main reflections typical of a fluorite-structured material with an fcc unit cell, corresponding to the (111), (200), (220), (311), (222), and (400) planes [21]. Note that La^{3+} shifts the CeO_2 characteristic peaks to lower angles, and the intensity of the peaks decreases with La^{3+} loading. This means that La^{3+} affects the crystal structure. This is in line with the conclusion of Raman spectroscopy characterisation. Comparison between the catalyst diffractograms and the La_2O_3 that is included as a reference in Fig. 6 confirms that La^{3+} is in the CeO_2 lattice. Characteristic La_2O_3 peaks are not observed in the La^{3+}-containing samples, even at high loading. This confirms that there is no segregation of phases in La^{3+}-containing catalysts.

The average crystallite sizes (D) of catalysts were determined with the Scherrer equation,

$$D = \frac{K \cdot \lambda}{\beta \cdot \cos\theta}$$

where λ is the X-ray wavelength, K is the particle shape factor, taken as 0.94 [18], β is defined as the width at half-maximum of the peak, and θ is the position (angle) of the peak. The average crystallite size of CeO_2 was estimated to be about 100 nm, and the La^{3+}-containing CeO_2 catalysts presented a crystallite size between 25 and 60 nm. He et al. [5] also reported that the average crystallite size decreases with doping of CeO_2–ZrO_2 solid solutions with Y^{3+} cations.

3.6. TAP experiments

We investigated the interaction between gas-phase O_2 and catalysts in an advanced TAP reactor by pulsing both pure nonlabelled (Fig. 7) and pure labelled O_2 (Fig. 8). The responses shown in the figures were normalised at all of the temperatures, and the total amount of oxygen obtained by integration and addition of the areas corresponding to the different oxygen species evolved is similar, indicating good mass balance of the system studied. The Ar response profiles were superimposed for comparison (curves in gray).

Fig. 7a shows the O_2 responses at different temperatures for the experiments carried out with CeO_2, and Fig. 7b shows the counterpart profiles for the experiments performed with CeO_2-5La. All of these responses were recorded once the steady-state regime was reached. It is assumed that there is no interaction between Ar and catalysts. Therefore, Ar profiles can be considered a reference, and the differences between Ar and O_2 peak shapes and/or the delay of the O_2 peak with regard to the Ar peak are attributed to the interactions between O_2 and the sample. Profiles in Figs. 7a and 7b indicate that there are no appreciable interactions between O_2 and the catalysts in the range of temperatures studied.

Figs. 8a and 8b show experimental results similar to those described in Fig. 7, but with labelled O_2. In accordance with observations from Fig. 7a, Fig. 8a confirms that there are no interactions between gas-phase labelled O_2 and CeO_2 in the range 200–500 °C. However, at 600 °C, part of the pulse (^{18}O–^{18}O) sticks to the catalyst, and nonlabelled O_2 (^{16}O–^{16}O) and scrambled molecules (^{16}O–^{18}O) evolve. At this moment, it is not possible to discriminate between surface or bulk adsorption. In this experiment, the only source of ^{16}O is the oxygen atoms on the catalyst, and, therefore, this finding demonstrates the exchange of oxygen between gas-phase molecular oxygen and the oxy-

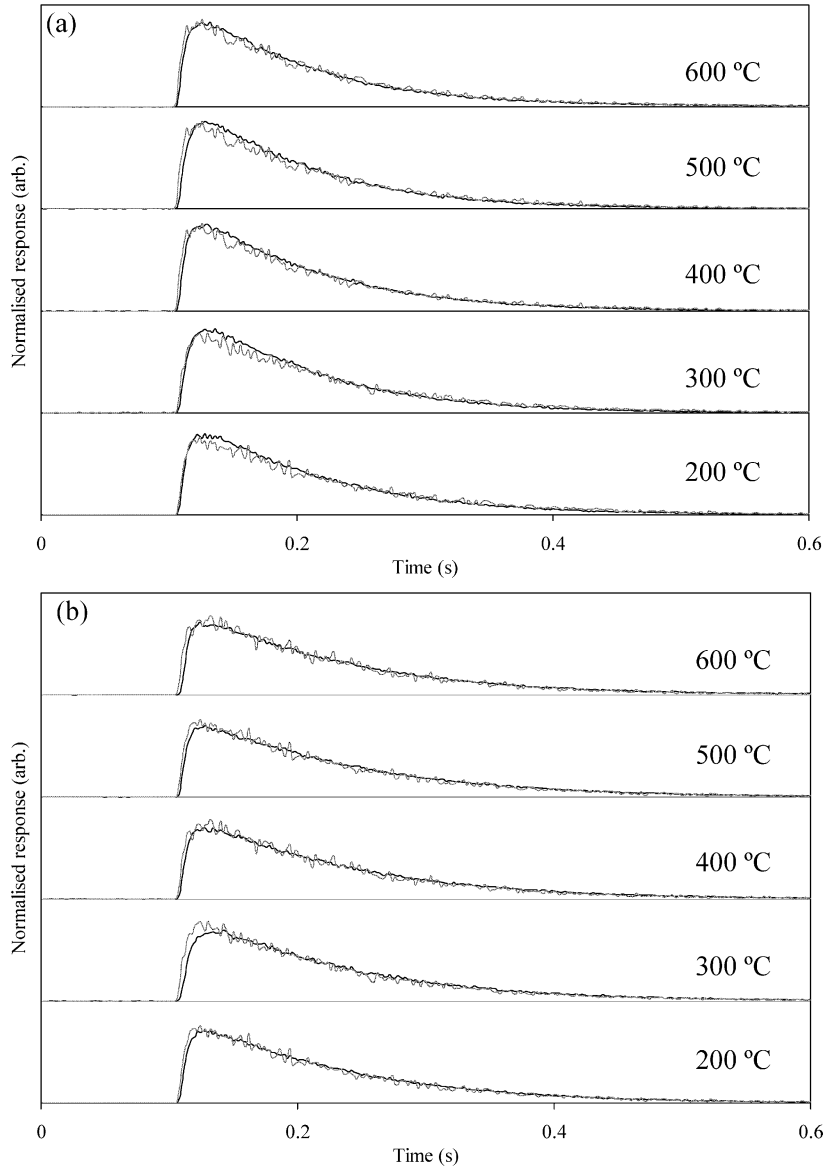

Fig. 7. TAP experiments with non-labelled O_2 pulsing. (a) CeO_2 and (b) CeO_2-5La. Grey lines-Ar (reference), black lines-O_2.

gen atoms on the lattice. He et al. [5] also observed oxygen exchange in solid solutions containing Zr, Y, and Ce or Pr in experiments performed in a flow microreactor. The fact that interactions were not observed with nonlabelled oxygen (Fig. 7) indicates that the exchange of oxygen occurs so quickly, and it is only detectable with labelled oxygen.

Fig. 8b, corresponding to $^{18}O_2$ exchange on the CeO_2-5La catalyst, also shows exchange of oxygen at 500 and 600 °C. If experiments described in Figs. 8a and 8b for similar temperatures (500 or 600 °C) are compared, the peak profiles indicate that La^{3+} favours the exchange of oxygen between gas phase and catalyst.

The mass balance in the experiments shown in Fig. 8 makes it possible to quantify the percentage of ^{18}O–^{18}O, ^{16}O–^{18}O, and ^{16}O–^{16}O that evolved in each experiment. Results compiled in the Table 2 indicate that, at 600 °C, about 40% of the pulsed ^{18}O–^{18}O sticks on the CeO_2 catalyst, and mainly ^{16}O–^{16}O evolves (37%), which has to be formed by recombination of two oxygen atoms from the lattice. A small amount of scrambled oxygen (3%) also evolves. For the CeO_2-5La catalyst at 600 °C, 72% of the labelled oxygen sticks and mainly ^{16}O–^{16}O is generated (64%). At 500 °C, the CeO_2-5La catalyst also exchanges more oxygen than CeO_2. Only the La^{3+}-containing sample shows oxygen exchange at 400 °C.

Fig. 9 shows the profiles corresponding to the labelled O_2 pulsed into the soot-catalyst mixtures. In these experiments O_2, CO, and CO_2 were monitored. Table 3 summarises the masses monitored (mass) and the assignment of these signals (gas). This table also compiles the percentage of each gas evolved at different temperatures, and the data corresponding to experiments performed with only soot are also included in Table 3.

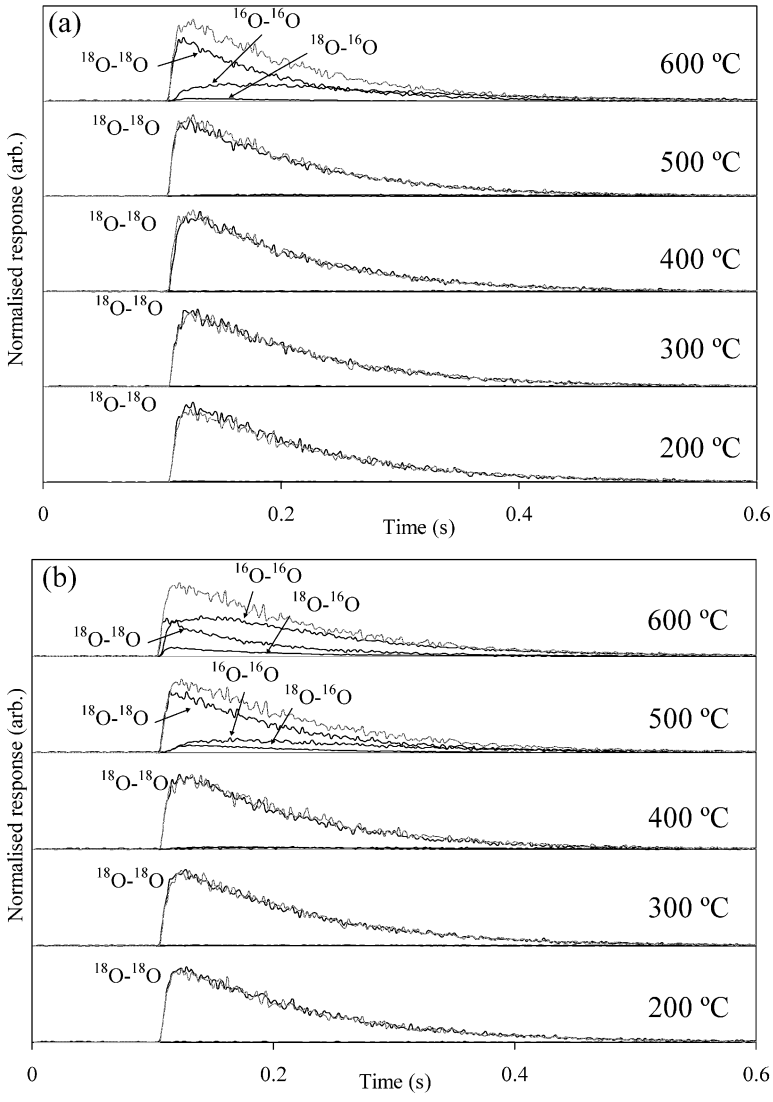

Fig. 8. TAP experiments with labelled O_2 pulsing. (a) CeO_2 and (b) CeO_2-5La. Grey lines-Ar (reference), black lines-non-labelled and labelled O_2 species.

With the use of soot-CeO_2 (Fig. 9a), at 200 and 300 °C, 100% pulsed labelled oxygen is measured. This indicates that there is no soot oxidation at these temperatures. However, above 400 °C, part or all of the labelled O_2 pulsed is consumed and CO and CO_2 are observed as reaction products of soot oxidation. At 600 °C, for example, the pulsed labelled O_2 is completely consumed, and CO and CO_2 are, respectively, 27 and 73% of the gas evolved. Note that both CO and CO_2 contained nonlabelled oxygen, which indicates that the labelled oxygen pulsed sticks to the catalyst, and the oxygen on the lattice reacts with soot. In the presence of catalyst the gas-phase labelled oxygen replaces nonlabelled lattice oxygen from CeO_2, creating highly active oxygen. This highly active nonlabelled oxygen reacts with soot, giving CO and CO_2.

Unlike in the absence of soot, where oxygen exchange starts above 500 °C (Table 2), in the presence of soot this highly active lattice oxygen is removed at temperatures as low as 400 °C (Table 3). Soot acts as a driving force in

Table 2
Percentage of gases evolved in TAP experiments with labelled O_2 pulses to CeO_2 and CeO_2-5La catalysts

Temperature (°C)	Gas	CeO_2 (%)	CeO_2-5La (%)
200	^{16}O–^{16}O	1	–[a]
	^{18}O–^{16}O	–	–
	^{18}O–^{18}O	99	100
300	^{16}O–^{16}O	–	–
	^{18}O–^{16}O	–	1
	^{18}O–^{18}O	100	99
400	^{16}O–^{16}O	1	3
	^{18}O–^{16}O	–	4
	^{18}O–^{18}O	99	93
500	^{16}O–^{16}O	4	25
	^{18}O–^{16}O	1	9
	^{18}O–^{18}O	95	66
600	^{16}O–^{16}O	37	64
	^{18}O–^{16}O	3	8
	^{18}O–^{18}O	60	28

[a] "–" not evolved.

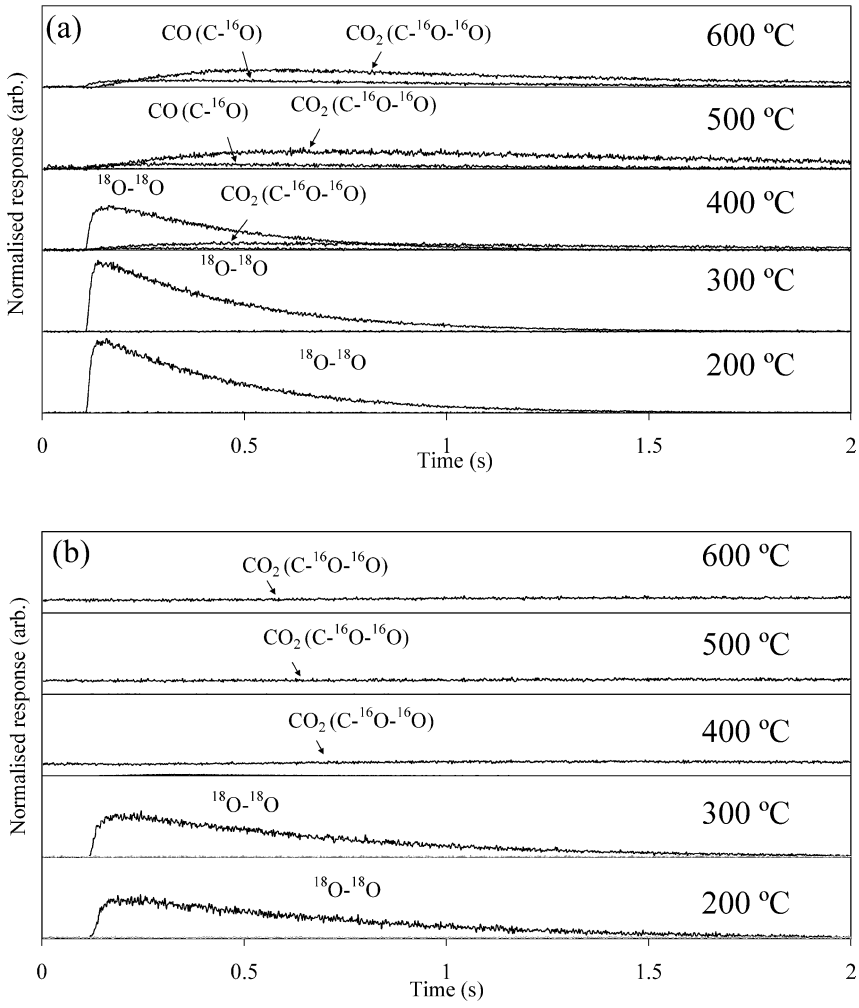

Fig. 9. TAP experiments with labelled O_2 pulsing. (a) soot + CeO_2 and (b) soot + CeO_2-5La.

Table 3
Percentage of gasses evolved in TAP experiments with labelled O_2 pulses to soot and soot-catalyst mixtures

Mass	Gas	Soot					Soot + CeO_2					Soot + CeO_2-5La				
		Temperature (°C)					Temperature (°C)					Temperature (°C)				
		200	300	400	500	600	200	300	400	500	600	200	300	400	500	600
48	CO_2 (C–^{18}O–^{18}O)	–[a]	–	–	1	4	–	–	–	–	–	–	–	–	–	–
46	CO_2 (C–^{16}O–^{18}O)	–	–	–	2	5	–	–	–	–	–	–	–	–	–	–
44	CO_2 (C–^{16}O–^{16}O)	–	–	–	1	2	–	–	32	85	73	–	–	98	100	100
36	O_2 (^{18}O–^{18}O)	100	100	100	89	71	100	100	63	–	–	100	100	2	–	–
34	O_2 (^{16}O–^{18}O)	–	–	–	–	–	–	–	–	–	–	–	–	–	–	–
32	O_2 (^{16}O–^{16}O)	–	–	–	–	–	–	–	–	–	–	–	–	–	–	–
30	CO (C–^{18}O)	–	–	–	2	13	–	–	–	–	–	–	–	–	–	–
28	CO (C–^{16}O)	–	–	–	5	5	–	–	5	15	27	–	–	–	–	–

[a] "–" not evolved.

the removal of this highly active oxygen, and the oxygen exchange temperature is decreased. As expected, the increase in temperature affected the CO/CO_2 ratio, and CO was progressively formed with temperature, in spite of the fact that CO_2 was the main carbon-containing product.

CeO_2-5La behaviour is qualitatively similar to that of CeO_2. However, above 400 °C, the pulsed labelled O_2 is completely consumed and CO_2 continuously evolves. In accordance with TGA experiments, these results indicate that the presence of La^{3+} in the CeO_2 lattice lowers the onset temperature of soot oxidation and improves the catalytic ac-

Table 4
Species involved in the redox cycles for the catalytic gasification of activated carbons by NO (from [22])

Metal catalyst	Reduced state (M_{red})	Oxidised state (M_{ox}–O)
Chromium	Cr_2O_3	CrO_2
Nickel	Ni	NiO
Cupper	Cu	CuO/(or Cu_2O)
Cobalt	Co (or CoO or Co_3O_4)	Co_2O_3
Calcium	CaO	CaO(O)
Potassium	K_xO_y	K_xO_{y+1}
Iron	Fe (or Fe_xO_y)	FeO (or Fe_xO_{y+1})

tivity. Moreover, La^{3+} also improves the selectivity towards CO_2 formation.

The noncatalysed reaction between soot and labelled oxygen proceeded in a manner different from that observed for CeO_2 and CeO_2-5La catalysed reactions. Data in Table 3 indicate that there was no reaction between soot and labelled O_2 below 400 °C, and at 500 and 600 °C part of the labelled oxygen is consumed. CO and CO_2 evolved at both of these temperatures. CO and CO_2 containing nonlabelled oxygen should be attributed to surface oxygen complexes on the carbon before reactions. However, ^{18}O-containing CO and CO_2 come from reactions with labelled oxygen.

4. Discussion

The results can be explained by considering the generally accepted mechanism for the catalytic oxidation of carbon, which is valid for many metal catalysts [22,23] including alkaline, alkaline earth, and transition metals. In this mechanism, the metal catalysts participate in a redox cycle, in which the metal is consecutively oxidised and reduced. The mechanism involves the following steps:

$$M_{red} + \text{gas-O} \rightarrow M_{ox}\text{–O}, \quad (1)$$

$$M_{ox}\text{–O} + C_f \rightarrow M_{red} + \text{SOC}, \quad (2)$$

$$\text{SOC} \rightarrow \text{CO or } CO_2, \quad (3)$$

where M_{red} and M_{ox}–O represent the reduced and oxidised states of the catalyst, respectively. Gas-O represents the oxidant gas (O_2, CO_2, H_2O, NO, NO_2, etc.), C_f denotes a carbon active site (or *free* site) on the carbon surface, and SOC represents a surface carbon–oxygen complex. In the first step, the catalyst "captures" oxygen from the gas-phase molecules and is itself oxidised. In the second step, the oxygen on the catalyst is transferred to an active site on the carbon surface, and the catalyst is reduced. In the third step, the SOC decomposes to yield CO or CO_2.

As an example, the redox pairs in Table 4 have been suggested to participate in the catalysed gasification of activated carbons by NO [22].

The large part of the reported literature related to rare earth catalysts based on studies focused on TWC application, and results included in this work indicate that the previously described mechanism also seems to be valid for soot oxidation under our experimental conditions. It is well known that in the CeO_2-containing catalyst designed for TWC, the redox pair Ce^{4+}/Ce^{3+} is the basis of the catalytic activity for CO and HC oxidation by NO_x and O_2. In brief, Ce^{3+} is oxidised by NO_x and/or O_2 to Ce^{4+}, which is reduced by CO and HC. Vidmar et al. [15] reported the important role of trivalent dopants in improving this redox process and are in agreement with our results.

Results presented in this study suggest that both CeO_2 and CeO_2-%La catalysts follow a Ce^{4+}/Ce^{3+} redox mechanism. The redox behaviour studied by TPR demonstrates the existence of Ce^{4+} cations that can be reduced to Ce^{3+}, and that La^{3+} favours this reduction process. TAP experiments show that the catalysts capture O_2 from the gas phase. Under high vacuum, in the absence of reductant species and once the lattice is saturated, the O_2 gas replaces oxygen atoms on the lattice, which are recombined and evolve again as O_2. This indicates that the redox cycle $Ce^{3+} \leftrightarrow Ce^{4+}$ is taking place. In the presence of soot (TGA and TAP experiments), it can be expected that the highly reactive oxygen atoms generated by the catalyst will not be recombined to yield O_2, but react with soot. We denote this lattice oxygen species as "active oxygen" because it is reasonable to assume a very high reactivity.

The rate of $^{18}O_2$ exchange with CeO_2 and the creation of active oxygen are much faster than the rate of $^{18}O_2$ direct reaction with soot. Similarly, the rate of active oxygen reaction with soot is much faster than the rate of its combination giving gas-phase O_2.

The incorporation of La^{3+} into the CeO_2 lattice significantly improves the generation of "active oxygen," which is deduced from the oxygen exchange data. The creation of such active oxygen species starts at 400 °C, thereby decreasing the soot oxidation temperature. CeO_2-5La produces more such active species, leading, for example, to 98% conversion of pulsed $^{18}O_2$ to CO_2 at 400 °C compared with 37% over CeO_2 alone (to CO and CO_2). Raman spectra indicate that this improvement is related to the deformation of the CeO_2 structure, which increases the oxygen mobility on the lattice and favours the $Ce^{4+} \leftrightarrow Ce^{3+}$ cycle. The generation of "active oxygen," induced by La^{3+}, explains the high activity of the CeO_2-%La catalysts in relation to CeO_2 alone, observed in TGA experiments under tight contact conditions. This improvement in soot conversion over La^{3+}-containing catalysts can only be attributed to the formation of solid solutions, as demonstrated by the lower activity over physically mixed $CeO_2 + La_2O_3$ catalyst (Fig. 1).

In the catalysed soot oxidation process, the surface area of the catalyst plays a crucial role because it is closely related to the gas-catalyst interactions. This is also the case for catalyst reduction by H_2, as deduced from the relationship between the onset temperature of H_2 consumption in TPR experiments and the BET surface area of catalysts as shown in Fig. 10.

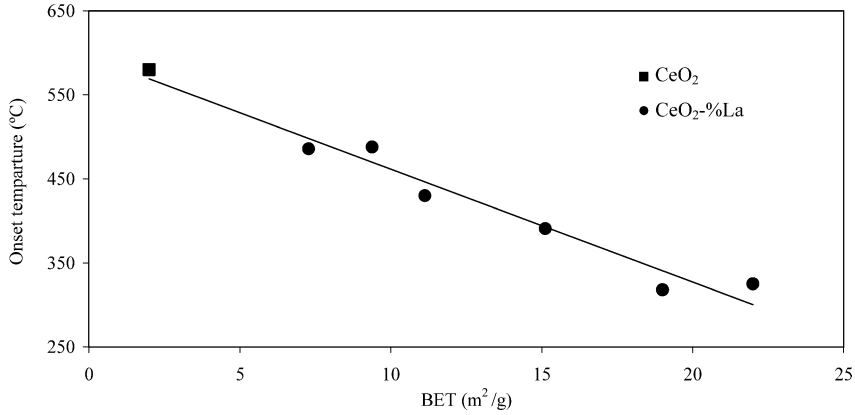

Fig. 10. Onset temperature of H_2 consumption in TPR versus BET surface area of the respective catalysts.

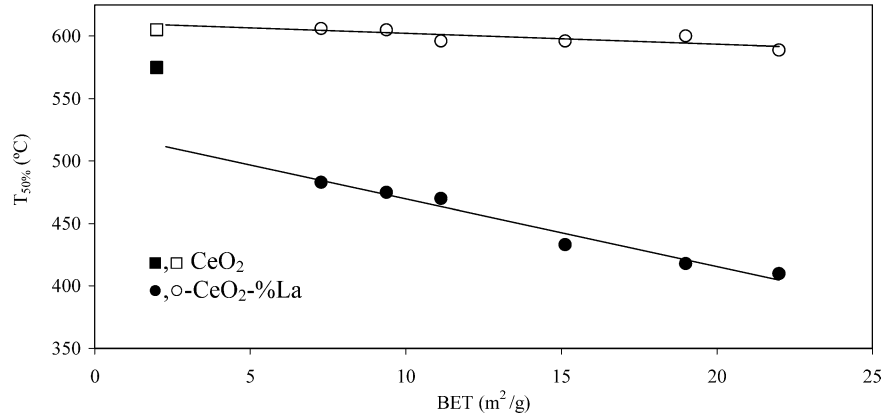

Fig. 11. $T_{50\%}$ of soot oxidation from TGA versus BET surface area of the respective catalysts. Open symbols: loose contact; solid symbols: tight contact.

In Fig. 11, the $T_{50\%}$ for soot oxidation is represented as a function of the BET surface area of the catalyst. A linear relationship is observed under both tight and loose contact conditions. The only exception is the CeO_2 catalyst in tight contact conditions, which does not display the expected trend. This suggests that the BET surface area is not the only factor affecting the activity of the catalysts, and active oxygen might play an important role. Under loose contact conditions, it seems appropriate to assume that most of the active oxygen generated by the catalyst is not useful for soot oxidation. Loose contact between catalyst and soot particles makes the "active oxygen" transfer to soot difficult, and the active species will be recombined to yield O_2 before they react with soot. Therefore, differences between CeO_2 and CeO_2-%La related to active oxygen participation are not observed, and BET surface area is the only factor that determines the activity of catalyst. However, the transport of active oxygen from catalysts to soot particles seems not to be a problem in tight contact conditions. Therefore, the La^{3+}-containing catalysts that generate "active oxygen" at lower temperatures and in major amounts are much more effective for soot oxidation. The participation of active oxygen in the reaction explains that CeO_2 is out of the linear trend (Fig. 11).

As we consider the results of this study, two challenges remain for future research: designing new materials that generate high amounts of active oxygen species, and determining the appropriate cations with which to dope CeO_2, which seems to be a promising route. Furthermore, it remains to design appropriate catalytic systems that improve the contact between soot and catalyst in order to favour the useful utilisation of active oxygen.

5. Conclusions

La^{3+} significantly improves the catalytic activity of CeO_2 for soot oxidation by O_2. The best results were obtained with 5 wt% La^{3+} catalyst in both loose and tight contact conditions. This improvement is related to the increase in the BET surface area, which improves the O_2–catalyst interaction, and to the change in the redox properties of the catalyst. Experiments performed with labelled O_2 demonstrate that gas-phase O_2 replaces oxygen atoms on the catalyst lattice. The amount of oxygen exchanged is improved by doping of CeO_2 with La^{3+}. La^{3+} also decreases the onset temperature of this process from 500 to 400 °C. The highly reactive active oxygen species generated by the catalyst during the O_2

exchange process are very active in soot oxidation. However, the lifetime of this species is very small, and it can only be transferred to the carbon particles in close vicinity, such as that achieved in tight contact conditions; otherwise they are recombined to generate O_2.

Acknowledgments

The authors thank the Spanish MEC for the fellowship of ABL and Engelhard Corporation for its financial support.

References

[1] J. Fenger, Atmos. Environ. 33 (1999) 4877.
[2] J.P.A. Neeft, M. Makkee, J.A. Moulijn, Fuel Process. Technol. 47 (1996) 1.
[3] H.S. Gandhi, G.W. Graham, E.W. McCabe, J. Catal. 216 (2003) 433.
[4] J. Kašpar, P. Fornasiero, M. Grazini, Catal. Today 50 (1999) 285.
[5] H. He, H.X. Dai, K.W. Wong, C.T. Au, Appl. Catal. A 251 (2003) 61.
[6] B.A.A.L. van Setten, M. Makkee, J.A. Moulijn, Catal. Rev.-Sci. Eng. 43 (2001) 489.
[7] T. Campenon, P. Wouters, G. Blanchard, P. Macaudiere, T. Seguelong, SAE Paper 2004-01-0071.
[8] A. Setiabudi, M. Makkee, J.A. Moulijn, Appl. Catal. B 50 (2004) 185.
[9] A. Setiabudi, M. Makkee, J.A. Moulijn, Appl. Catal. B 42 (2003) 35.
[10] A. Setiabudi, J. Chen, G. Mul, M. Makkee, J.A. Moulijn, Appl. Catal. B 51 (2004) 9.
[11] V.G. Milt, C.A. Querini, E.E. Miró, M.A. Ulla, J. Catal. 220 (2003) 424.
[12] M.L. Pisarello, V. Milt, M.A. Peralta, C.A. Querini, E.E. Miró, Catal. Today 75 (2002) 465.
[13] B.A.A.L. van Setten, J.M. Schouten, M. Makkee, J.A. Moulijn, Appl. Catal. B 28 (2000) 253.
[14] C.E. Hori, H. Permana, K.Y.S. Ng, A. Brenner, K. More, K.M. Rahmoeller, D. Belton, Appl. Catal. B 16 (1998) 105.
[15] P. Vidmar, P. Fornasiero, J. Kašpar, G. Gubitosa, M. Grazini, J. Catal. 171 (1997) 160.
[16] G.L. Markaryan, L.N. Ikryannikova, G.P. Muravieva, A.O. Turakulova, B.G. Kostyuk, E.V. Lunina, V.V. Lunin, E. Zhilinskaya, A. Aboukais, Colloids Surfaces A 151 (1991) 435.
[17] A. Nineshige, T. Taji, Y. Muroi, M. Kobune, S. Fujii, N. Nishi, M. Inaba, Z. Ogumi, Solid State Ionics 135 (2000) 481.
[18] L.N. Ikryannikova, A.A. Aksenov, G.L. Markayan, G.P. Muravieva, B.G. Kostyuk, A.N. Kharlanov, E.V. Linina, Appl. Catal. A 210 (2001) 225.
[19] M. Fernandez-García, A. Martínez-Arias, A. Iglesias-Juez, C. Belver, A.B. Hungría, J.C. Conesa, J. Soria, J. Catal. 194 (2000) 385.
[20] P. Fornasiero, J. Kašpar, M. Grazini, J. Catal. 167 (1997) 576.
[21] D. Terribile, A. Trovarelli, J. Llorca, C. de Leitenburg, G. Dolcetti, Catal. Today 43 (1998) 79.
[22] M.J. Illán-Gómez, A. Linares-Solano, L.R. Radovic, C. Salinas-Martínez de Lecea, Energy Fuels 10 (1996) 158.
[23] J.A. Moulijn, F. Kapteijn, Carbon 33 (1995) 1155.